JOURNAL OF THERMOPHYSICS AND HEAT TRANSFER
Vol. 22, No. 3, July–September 2008

Effect of Temperature-Sensitive-Paint Thickness on Global Heat Transfer Measurement in Hypersonic Flow

H. Nagai,* S. Ohmi,† and K. Asai‡
Tohoku University, Sendai 980-8579, Japan
and
K. Nakakita§
Japan Aerospace Exploration Agency, Tokyo 182-8522, Japan

DOI: 10.2514/1.34152

Heat flux measurement in a hypersonic wind tunnel is one of the necessary requirements for designing the next-generation reentry vehicle. Heat flux is usually calculated from a temporal change in temperature on a model surface. Temperature-sensitive paint provides a global temperature measurement technique based on photochemical reaction. This technique was applied to a hypersonic shock tunnel test, but there were uncertainties caused by the thickness of the temperature-sensitive-paint layer. In this study, the relationship between the temperature-sensitive-paint layer thickness and the measurement accuracy of heat flux was investigated. The models were tested at Mach 10 in the Japan Aerospace Exploration Agency's 0.44-m hypersonic shock tunnel and the heat flux, caused by aerodynamic heating on the model surface, was measured. A comparison between temperature-sensitive-paint data and conventional thermocouple data showed that the measurement error changed with the paint layer thickness. Then a three-dimensional wing–body model was tested to demonstrate the validity of temperature-sensitive paint of an optimized thickness, and a complicated heat flux pattern caused by the shock wave/shock-wave interaction was observed.

Nomenclature

C	=	constant in Eq. (3)
c	=	specific heat of the model material
D	=	diameter of the model
E	=	activation energy
h	=	thickness of the temperature-sensitive-paint layer
I	=	luminescent intensity
I_a	=	absorbed light intensity
K_T	=	temperature-sensitive-paint calibration constant
k_D	=	kinetic constant of nonradiative decay
k_L	=	rate constant for radiative decay
k_0	=	rate constant in Eq. (2) with no temperature dependence
k_1	=	rate constant in Eq. (2) with temperature dependence
L	=	length of the model
n_{peref}	=	number of collected photoelectrons
q	=	heat flux
R	=	universal gas constant
T	=	temperature
$T_{\min}$	=	minimum resolvable temperature difference of the temperature-sensitive paint
t	=	time
x	=	distance from the leading edge of a wing at the root
α	=	angle of attack
β	=	angle of sideslip
ΔT	=	temperature rise from the steady state
κ	=	thermal conductivity
ρ	=	density of the model material
Φ	=	quantum efficiency

Subscripts

ref	=	reference condition
tc	=	temperature rise measured by a thin thermocouple

Presented as Paper 1048 at the 44th AIAA Aerospace Sciences Meeting and Exhibit, Reno, Nevada, 9–12 January 2006; received 20 August 2007; revision received 25 February 2008; accepted for publication 25 February 2008.

*Assistant Professor, Department of Aerospace Engineering. Member AIAA.
†Department of Aerospace Engineering; currently Employee, Mitsubishi Heavy Industry.
‡Professor, Department of Aerospace Engineering. Associate Fellow AIAA.
§Senior Researcher, Institute of Aerospace Technology, Chofu. Member AIAA.

I. Introduction

AERODYNAMIC heating is one of the most important challenges in the development of hypersonic flight vehicles. Both the type of thermal protection system and its weight are determined by the heat flux data provided from wind-tunnel tests and/or computational fluid dynamics (CFD) results. In wind-tunnel tests, various types of conventional thermal sensors are used to measure the quantitative heat flux [1–3]. They are all point sensors capable of measuring the heat flux only at spatially discrete points. Hypersonic flow includes many high local heat flux phenomena, such as shock wave/shock-wave interaction, shock wave/boundary-layer interaction, and boundary-layer transition. With conventional sensors, there is a possibility of failing to measure local heat flux peaks. Recently, various global heat flux measurement techniques have been developed and applied to wind-tunnel tests [4–6]. These techniques use a camera system to collect temperature distribution images. Temperature-sensitive paint (TSP) is one of the most promising options for global temperature distribution measurement, which is an optical temperature measurement technique based on the photochemical reaction of luminescent molecules. There are several studies involving TSP application in hypersonic wind tunnels [7–9]. In these studies, the heat flux was calculated using a steady thermal conduction or constant heat transfer coefficient. Nakakita et al. [10] demonstrated TSP's validity by applying it to global heat flux measurement in a short duration hypersonic shock tunnel. Furthermore, they acquired both a Japanese and an American patent for heat flux measurement using TSP [11,12]. However, the relationship between the thickness of the TSP layers and the measurement accuracy of heat flux has not been investigated in

detail. It is important because the TSP layer acts like an insulator, which increases the surface temperature detected by the TSP, which in turn causes a measurement error. Therefore, it is necessary to reduce the TSP layer's thickness to reduce the measurement error. Such a thin film of paint produces a very low signal-to-noise ratio (SNR) because the number of photons detected by a camera is reduced with a thinner film. In addition, the dye concentration of TSP affects the temperature sensitivity and the SNR. Thus, the relationship between the thickness of TSP layers and the measurement accuracy of heat flux should be investigated in detail.

In the present paper, the TSP properties were initially investigated with a focus on various conditions such as dye concentration, thickness, and thermal sensitivity in the sample test using a calibration chamber. Then, the relationship between the TSP layer thickness and the measurement accuracy of heat flux was investigated using a cylinder model, which was tested at Mach 10 in the Japan Aerospace Exploration Agency's (JAXA) 0.44-m hypersonic shock tunnel. Finally, the validity of the assertion that the optimal thickness of the TSP layer has little influence on the heat flux measurement error was demonstrated by measuring a heat flux distribution on a more complicated, three-dimensional wing–body model.

II. Theory

A. Temperature-Sensitive Paint

TSP [13,14] is a coating that consists of sensor molecules dispersed in a polymer binder. Figure 1 shows a schematic illustration of TSP measurement and an energy-level diagram of TSP molecules. When illuminated by light at an appropriate wavelength, the sensor molecules become electronically excited to an elevated energy state. The molecules undergo transition back to the ground state by one of several mechanisms, each of which occurs at a different rate. The predominant mechanisms are radiative decay (luminescence) and nonradiative decay through the release of heat. A part of nonradiative decay depends on the temperature. Therefore, the luminescence of the TSP coating decreases as the temperature increases.

The quantum efficiency of luminescence decreases as the temperature increases. This effect is known as "thermal quenching." In general, the quantum efficiency, Φ, is shown by

$$\Phi = I/I_a = k_L/(k_L + k_D) \tag{1}$$

where I is the luminescent intensity, I_a is the absorbed light, and k_L is the rate constant of radiative decay.

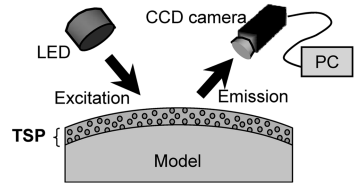

a) TSP measurement

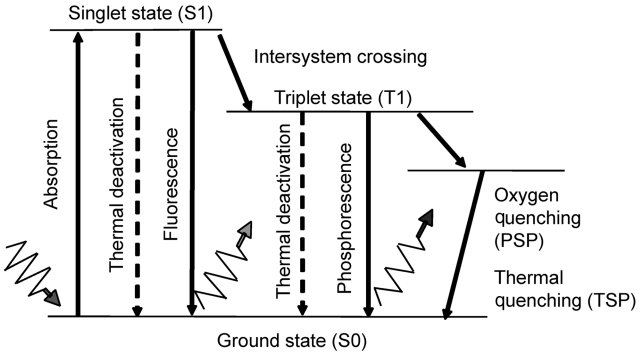

b) Energy-level diagram

Fig. 1 Schematic illustration of the TSP measurement and an energy-level diagram of TSP molecules.

The kinetic constant of nonradiative decay, k_D, is shown by

$$k_D = k_0 + k_1 \tag{2}$$

where k_0 and k_l are the rate constants without and with temperature dependence, respectively.

Using Arrhenius' model, k_1 is expressed by

$$k_1 = C\exp(-E/RT) \tag{3}$$

The intensity of the luminescence is proportional to the quantum efficiency. Thus, the relationship between the luminescence of TSP and the temperature is expressed by transforming Eqs. (1–3):

$$\ell_n \frac{I}{I_{\text{ref}}} = \frac{E_{\text{nr}}}{R}\left(\frac{1}{T} - \frac{1}{T_{\text{ref}}}\right) \tag{4}$$

where I_{ref} and T_{ref} are the luminescent intensity and temperature, respectively, obtained at a reference condition such as a wind-off state. E_{nr} is the activation energy for the nonradiative process, and R is the universal gas constant. Equation (4) indicates that, as the activation energy of the luminophore is increased, the thermal sensitivity of TSP increases. In theory, temperature is calculated by Eq. (4). However, in practical cases, it is convenient to use the following empirical equation:

$$\frac{I}{I_{\text{ref}}} = \sum_{k=0}^{n}\left\{a_k\left(\frac{T}{T_{\text{ref}}}\right)^k\right\} \tag{5}$$

The intensity, I, measured at a desired test condition is then used to calculate the temperature, T. The coefficient, a_k, can be obtained through calibration tests.

B. Calculation of Heat Flux

Assuming a semi-infinite body, as shown in Fig. 2, a temperature change at the surface is governed by the following classical heat conduction equation:

$$\begin{aligned} &\frac{\partial T}{\partial t} = \frac{k}{\rho c}\frac{\partial^2 T}{\partial x^2} \\ &q = -k\frac{\partial T}{\partial x} \quad \text{at} \quad x = 0 \\ &T = 0 \qquad\quad \text{at} \quad x = \infty \end{aligned} \tag{6}$$

The surface temperature at time t is reduced using Eq. (6):

$$T = \frac{1}{\sqrt{\pi}\sqrt{\rho c k}}\int_0^t \frac{q(t)}{(t-\tau)^{1/2}}\,\mathrm{d}\tau \tag{7}$$

The heat flux at time t can be calculated by transforming Eq. (7):

$$q(t) = \sqrt{\frac{\rho c k}{\pi}}\left[\frac{T(t)}{\sqrt{t}} + \frac{1}{2}\int_0^t \frac{(T(t) - T(\tau))}{(t-\tau)^{3/2}}\,\mathrm{d}\tau\right] \tag{8}$$

Finally, Eq. (8) is discretized by regarding the local linearization approximation of $T(t)$ [1], where the following equation is obtained:

$$q(t) = \frac{2\sqrt{\rho c k}}{\sqrt{\pi}}\left[\sum_{i=1}^{n}\frac{T(t_i) - T(t_{i-1})}{\sqrt{t_n - t_i} + \sqrt{t_n - t_{i-1}}}\right] \tag{9}$$

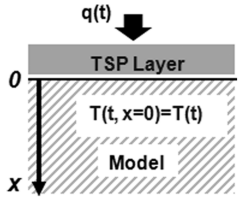

Fig. 2 One-dimensional heat conduction model assumed by a semi-infinity body.

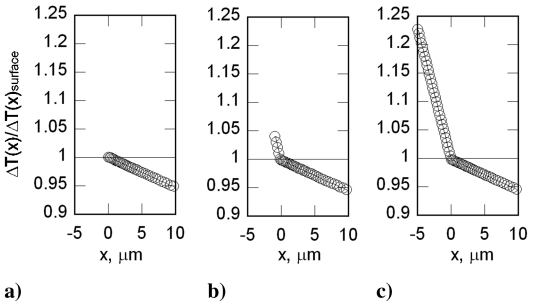

Fig. 3 Result of a one-dimensional thermal analysis that considered the TSP layer thickness: a) without TSP layer, b) 1 μm, and c) 5 μm. Temperature distributions at $t = 30$ ms after heating. $x > 0$: ceramics (Macor®), $x < 0$: polymer.

The incremental surface temperature measured by TSP is converted to the heat flux using Eq. (9) [2].

For TSP measurement, the model surface is covered by a thin layer of TSP that has thermal properties different from those of the model material. Consequently, a temperature measured by TSP is different from the model substrate temperature. Therefore, an error is included in the temperature measured by TSP and the heat flux calculated using Eq. (9). Figure 3 shows the results of a one-dimensional thermal analysis that considered the TSP layer thickness. This graph shows the difference in the temperature increase between the test model with a TSP layer and the test model without a TSP layer (only a substrate of the ceramic) [10]. In computation, the typical polymer properties ($\kappa = 0.2$ W/(m · K), $c = 1.2$ kJ/(kg · K), and $\rho = 1200$ kg/m^3) were used along with the TSP. As can be seen from this figure, the temperature measurement error increases as the thickness of the TSP increases. In the case of a TSP layer thickness of 5 μm, the temperature difference between the TSP surface and the model surface is 23%. Hence, a thinner layer of TSP is desirable from the viewpoint of temperature error, but is not desirable from the viewpoint of signal-to-noise ratio, because the luminescence intensity decreases as the TSP layer becomes thin and the number of sensor molecules decreases. Consequently, it is important to trade off between a measurement error caused by the TSP layer and the signal-to-noise ratio.

III. Sample Test

Sample tests were done to investigate the properties of TSP for various conditions such as dye concentration, layer thickness, and thermal sensitivity. The tests were conducted in a test chamber in which the temperature could be controlled by a Peltier device.

A. Temperature-Sensitive-Paint Formulation

The TSP used for this test employed a dichlorotris(1,10 phenanthroline)ruthenium(II) hydrate, or $Ru(phen)_3^{2+}$, as a probe molecule and polyacrylic acid as a polymer binder. $Ru(phen)_3^{2+}$ is known to have a high temperature sensitivity near room temperature. The peak absorbance of this luminophore is at wavelengths of approximately 350 and 430–450 nm, and the emission peak is 610 nm. The luminophore and the binder were dissolved in ethanol. The concentration of $Ru(phen)_3^{2+}$ with respect to the volume of polyacrylic acid varied from 10^{-3} to 10^{-1} mol/l. The TSP was sprayed on a 34 mm × 34 mm flat plate made of machinable glass ceramic. This is the same material that was used for the model in the wind-tunnel tests. A part of the sample plate was covered with masking tape to resemble an actual TSP layer whose thickness could be measured. The paint layer thickness was controlled by changing the number of spray strokes used to apply the TSP.

B. Experimental Setup

A sample plate was mounted on a Peltier device in a test chamber, and the temperature was controlled by a high accuracy (0.1% of the full span) thermoregulator whose temperature range was from −40 to 80°C. The chamber pressure was also controlled by using a pressure regulator (Druck Limited, DPI 515).

A confocal laser scanning microscope was used to measure the thickness of each TSP layer on the sample plate. The spatial resolution of the microscope was 0.01 μm and the A/D resolution was 12 bit. Figure 4 shows an example of the edge image of the TSP layer on the sample plate as scanned by the confocal laser scanning microscope. The layer thickness was determined from the difference in height between the TSP layer and the base plate.

The optical system for the sample tests is shown in Fig. 5. Two sets of light-emitting diodes with a peak wavelength of 470 nm were used as the excitation light source for the TSP. The luminescence form for the sample was captured by a thermoelectrically cooled charge-coupled device (CCD) camera (Hamamatsu ORCA-ER, C4742-95) with a 1024 × 1024 pixel resolution and 12-bit A/D resolution through a high-pass filter of cutoff wavelength at $\lambda = 580$ nm.

C. Experimental Conditions

Initially, the pressure sensitivity of the TSP was investigated. Then, two types of tests were conducted to evaluate the effects of the dye concentration and layer thickness and its thermal sensitivity. In both tests, the dye concentration varied among 10^{-3}, 10^{-2}, and 10^{-1} mol/l. The TSP layer thickness was changed from 0.3 to 10.0 μm. The total number of tested samples was 19 pieces.

When measuring the luminescent intensity of TSP samples, the temperature was kept at 20°C. The exposure time of the CCD camera was changed from 592 to 2293 μs to adjust the input light level near the full capacity of the CCD. The measured intensity was normalized by the exposure time for each sample plate to compare their relative intensities. When measuring the thermal sensitivity, the temperature of the sample was varied from 25 to 40°C at 5°C intervals. The pressure was kept at 100 kPa.

D. Results

Figure 6 shows the results of the pressure sensitivity of the TSP sample. The horizontal axis is the pressure and the vertical axis is the

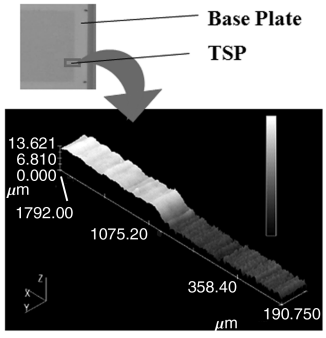

Fig. 4 Example of the edge image of the TSP layer on a sample plate scanned by the confocal laser scanning microscope.

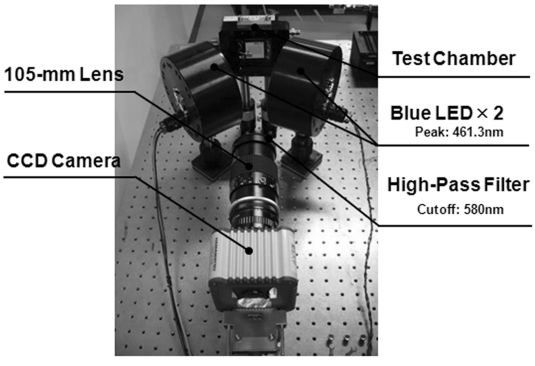

Fig. 5 Optical setup for the sample test.

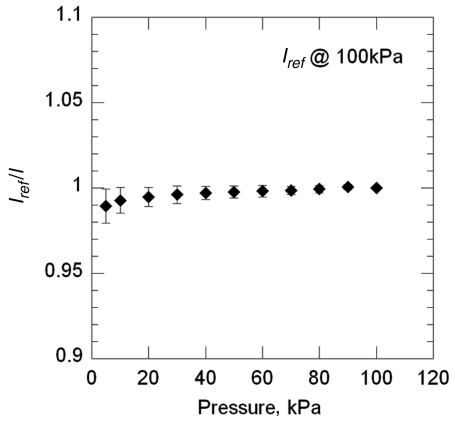

Fig. 6 Pressure sensitivity of TSP.

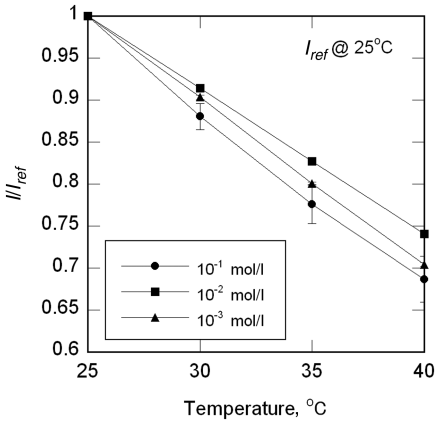

Fig. 8 Thermal sensitivity for dye concentration.

luminescent intensity ratio normalized by the value at 100 kPa. The figure shows that the pressure sensitivity of TSP does not depend on pressure. Consequently, the pressure dependency of the luminescence intensity was disregarded in the following discussions.

Figure 7 shows the results of the luminescent intensity test for TSP layer thickness. The horizontal axis is the TSP layer thickness measured by the confocal laser scanning microscope. The vertical axis is the luminescence intensity from TSP normalized by the corresponding exposure time. Three data sets with different dye concentrations are plotted. For the lowest dye concentration of 10^{-3} mol/l, the luminescent intensity increased as the thickness of the TSP increased. In the case of the dye concentration of 10^{-2} mol/l, the luminescent intensity level was the highest. For the highest dye concentration of 10^{-1} mol/l, the intensity level of TSP luminescence was smaller than that of the lower concentrations and the intensity level hardly changed even when the thickness of the TSP was increased. It is estimated that this result was caused by "self-quenching" [14–16]. Self-quenching is a phenomenon whereby the luminescence gets weaker as the dye concentration is increased due to the energy transfer among dye molecules. Usually, a TSP with higher concentrations emits luminescence with greater intensity. However, if the concentration exceeds a certain threshold, the luminescence starts to decrease. This means that the distances between the luminophore molecules are close and may vibrate (rovibronic excitation) with a greater amplitude, thus producing nonelastic energy transfer via intra- or intermolecular processes without emitting luminescence. In our experiment, the dye concentration threshold was expected to be around 10^{-2} mol/l.

Figure 8 shows the test results of the thermal sensitivity for various dye concentrations. The horizontal axis is the temperature and the vertical axis is the intensity ratio normalized by the value at 25°C. As can be seen in Fig. 7, the thermal sensitivity is dependent on TSP concentration. The thermal sensitivities for the dye concentrations of 10^{-1}, 10^{-2}, and 10^{-3} mol/l were 2.2, 2.0, and 1.7% per degree, respectively.

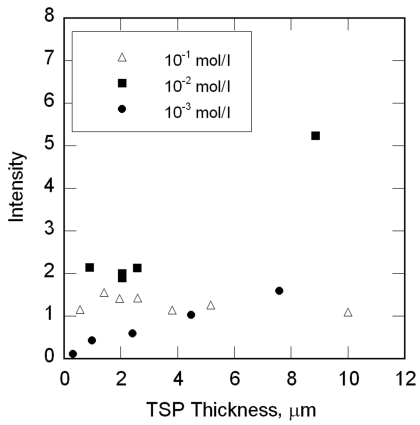

Fig. 7 Luminescent intensity with the TSP layer thickness.

Figures 9a–9j show the surface images of the TSP layer and the base plate on a sample plate scanned by the confocal laser scanning microscope. The conditions of each sample are shown in Table 1. The observation region of all images was 256 × 192 μm except for Fig. 9c, which was 768 μm × 576 μm.

In Figs. 9a–9i, the surface of the TSP was nonuniform and a lot of holes were open in almost all cases. The proportion of the holes in the surface area decreased as the thickness of the TSP increased. In the cases of Figs. 9f and 9i, with a thickness of 5.0 μm, the hole was hardly visible. In addition, there were rough surfaces in the base plate in Fig. 9j.

Finally, it is assumed that the best dye concentration could be determined from these results. Liu and Sullivan [17] discussed the uncertainty of the TSP measurement. According to their analysis, the minimum resolvable temperature difference $\Delta T_{\min}$ for the TSP is inversely proportional to the square root of the number of collected photoelectrons, n_{peref}, and approximately proportional to a constant K_T for the TSP, as shown in Eq. (10):

$$(\Delta T_{\min}) = \frac{K_T}{\sqrt{(n_{\text{peref}})_{\max}}}\left[1 + \exp\left(\frac{T - T_{\text{ref}}}{K_T}\right)\right]^{1/2} \tag{10}$$

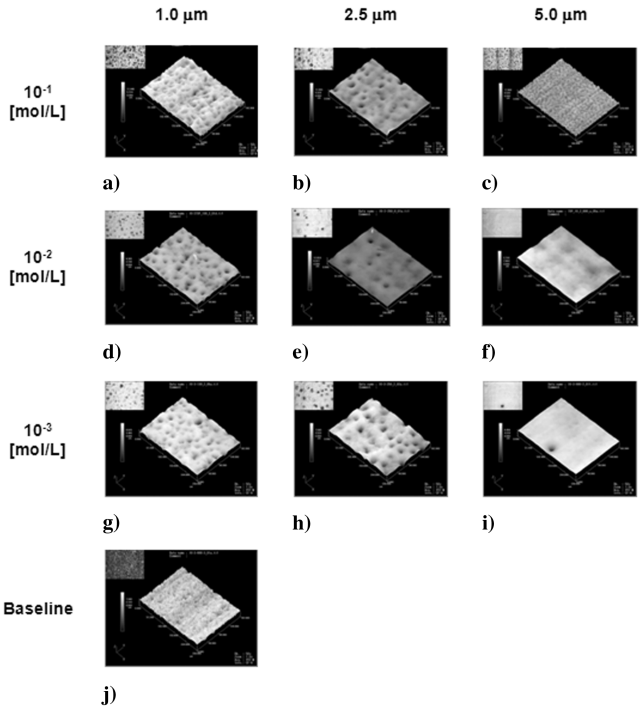

Fig. 9 Surface images of the TSP layer and base plate on a sample plate scanned by the confocal laser scanning microscope.

Table 1 Conditions of the surface images

Case	Dye concentration, mol/l	TSP thickness, μm
a		1.0
b	10^{-1}	2.5
c		5.0
d		1.0
e	10^{-2}	2.5
f		5.0
g		1.0
h	10^{-3}	2.5
i		5.0
j	Base plate	

where K_T is a TSP calibration constant with a temperature unit, defined as $K_T = (T - T_{\text{ref}})/\ell_n(I/I_{\text{ref}})$.

When the optical condition is the same, Eq. (10) can be rewritten in the following manner by using luminescence intensity, I:

$$(\Delta T_{\min}) \propto \frac{K_T}{\sqrt{I}} \tag{11}$$

This means that the minimum resolvable temperature difference for the TSP is proportional to K_T of the calibration constant and is inversely proportional to the luminescence intensity.

Using the data in Figs. 7 and 8, the minimum resolvable temperature difference was the smallest for 10^{-2} mol/l and the largest for 10^{-3} mol/l. Therefore, the TSP with a dye concentration of 10^{-2} mol/l was chosen to be applied for the wind-tunnel tests.

IV. Wind-Tunnel Tests

To evaluate the effect of TSP layer thickness on heat transfer measurement in hypersonic flow, wind tunnel tests were conducted in a short duration hypersonic shock tunnel. Two types of test models were used in this study. First, a two-dimensional cylinder model was used to investigate the relationship between the thickness of the TSP layer and the measurement error in the temperature. Then, a three-dimensional wing–body model was used to demonstrate the validity of the TSP technique for complicated flow.

A. Experimental Facility

In this study, the JAXA 0.44-m hypersonic shock tunnel was used, as shown in Fig. 10. The shock tunnel consisted of both a high- and a low-pressure tube. The high-pressure tube, which was located at the end of the low-pressure tube and arranged with the low-pressure tube, part of which was contained inside of it, was 5.2 m in length and 0.318 m in diameter. The low-pressure tube had a diameter of 74 mm and a length of 27.8 m. The first quick valve, located at the low-pressure tube's initial end, was operated by high-pressure air. The second quick valve, located at the end of the low-pressure tube, was electronically operated. Air compressed and heated by a shock was discharged into a vacuum chamber through the Mach 10 contoured nozzle. The exit diameter of this nozzle was 0.44 m.

There were two operational modes for this shock tunnel: one was the long-duration mode and the other was the high-enthalpy mode. In this study, we employed a long-duration mode that has a flow duration on the order of 10 ms. The performance of the facility for the long-duration mode was as follows. The total temperature T_0 was about 1180 K and the pitot pressure at the test section was 8800 Pa. The flow Mach number was 10.4 and the unit Reynolds number was 1.55×10^6 m^{-1}. The flow duration was from 30 to 50 ms.

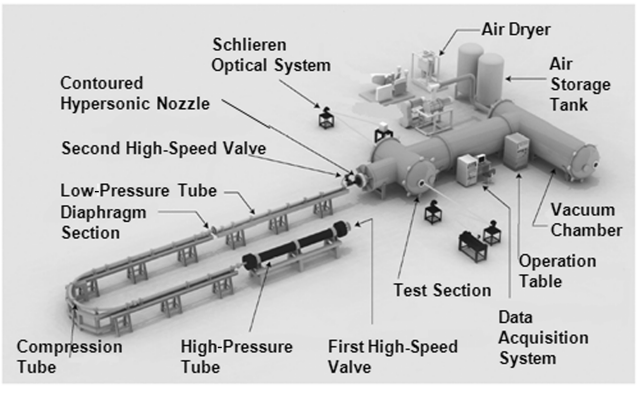

Fig. 10 JAXA 0.44-m hypersonic shock tunnel.

B. Test Models

The test models were made of machinable glass ceramic. This material was selected because of its relatively low heat conductivity, which means that the dissipation of heat in the model is minimized. Figure 11 shows a photograph of the cylinder model. The length of the model, L_1, was 100 mm and the diameter, D_1, was 20 mm. Two thin-film thermocouple sensors made of Cu and Ni were at the center of the model to compare the heat flux measured by the TSP. The accuracy of the thin thermocouple was about 1.0% of the full scale obtained by the in situ calibration. The sensing area of the thermocouple was about 0.3 mm × 0.3 mm and the thickness was about 0.3 μm. For the cylinder model, TSP was applied on the upper half of the model. Shown in Fig. 10, the upper region was divided into three parts, in which there were TSP layers of three different thicknesses, A, B, and C. The spanwise width of each TSP layer was 10 mm. The area 15 mm from the top of the model was not painted with TSP because the flow over this region was distorted by the end of the model. The registration marks for the image processing were painted with the black dots at the top and bottom boundaries. Figure 12 shows a photograph of the wing–body model. The length of this model, L_2, was 200 mm and the fuselage diameter, D_2, was 28 mm. The sweepback angle of the wing was 55 deg. This model represented a typical reentry vehicle configuration, and the obtained results would be useful in discussing the merits and demerits of the TSP technique when used for future practical wind-tunnel tests.

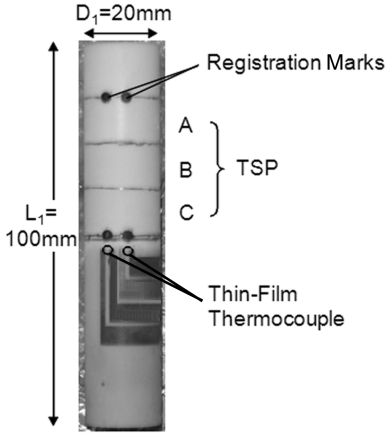

Fig. 11 Photograph of the two-dimensional cylinder model.

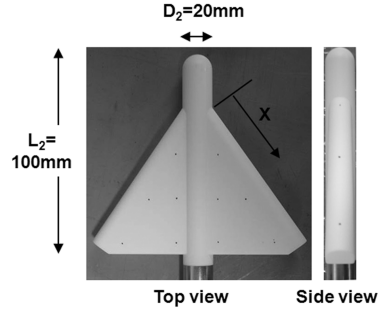

Fig. 12 Photograph of the three-dimensional wing–body model.

Based on the results of the sample tests, TSP with a luminophore/binder concentration of 10^{-2} mol/l was used in the wind-tunnel tests. TSP was sprayed on the model surfaces using an air compressor. The pressure of the spray nozzle was kept constant using a pressure regulator. The thickness of the TSP layer was controlled by changing the number of spray strokes. It was difficult to measure the TSP thickness on the model when using the laser microscope because the model had curvature. Therefore, when TSP was sprayed on a cylinder model, a flat sample plate, which was placed near the model, was also painted at the same time. The thickness of the layer on this sample plate was measured by the confocal laser scanning microscope and used as a measure of TSP layer thickness on the model.

The thickness of the TSP layer for the wing–body model was determined based on the results of the cylinder model tests. In the cylinder model tests, the thickness of the TSP layer was estimated using a sample plate, and the uniformity was evaluated, by eyesight, by observing the color of the TSP layer.

C. Optical Setup

The optical setup for the wind-tunnel tests is shown in Fig. 13. A powerful continuous Ar laser (Spectra Physics Stabilite 2017) was used as an excitation light source. The wavelength of the laser light was 454.5–514.5 nm, which was suitable for exciting our TSP. Because the laser is coherent light, no illumination filter was used. The total power of this laser was 6 W, which allowed us to increase the luminescent intensity from the TSP layer. The output of the Ar laser was guided into a liquid light guide and transferred near the optical window. The laser beam was collimated using the lens and illuminated the test model. A mechanical shutter was used to minimize the time that the model was exposed to the laser light because using a powerful laser can lead to saturation effects.

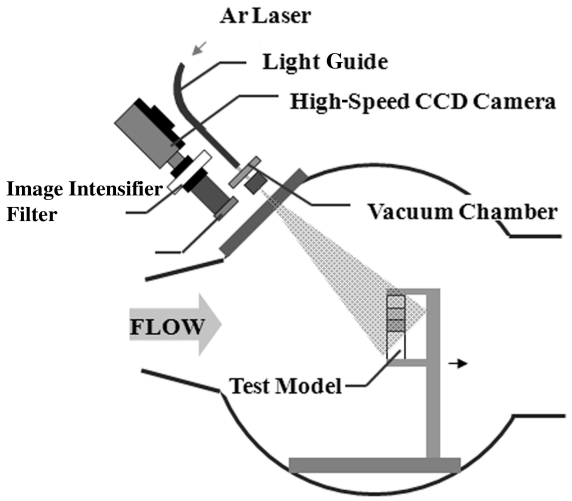

Fig. 13 Schematic illustration of the measurement system.

To detect the luminescence from the TSP, a high-speed CCD video camera (Shimadzu HVC-2S) was used. This camera allowed us to measure a temporal change in the TSP luminescent intensity in a short duration of the shock tunnel. The high-speed video camera can record up to one million frames per second (number of images, 103 shots) and has a high spatial resolution (312 × 260 pixels) at all recording speeds with a 10-bit A/D resolution, which is necessary for quantitative temperature measurement.[¶] The CCD camera has high linearity in the intensity and homogeneity of CCD elements as shown in Fig. 14.

In this study, the frame rate was set at 1 kHz. A set of 103 images was acquired in a long duration of 50 ms. To amplify the intensity image of luminescence from the TSP, an image intensifier (Hamamatsu C7786) was installed in front of the CCD camera. Because an image intensifier would degrade the spatial resolution of the measured optical images, the gain of the intensifier was kept at the lowest value for each case. A camera lens with an optical filter was placed in front of the image intensifier. A 200-mm long distance lens was used for the cylinder model tests, and an 85-mm lens was used for the wing–body tests. The optical filter was a long pass filter with a cutoff wavelength at 532 nm to prevent any reflected Ar laser light from entering the camera.

The TSP calibration for the cylindrical and wing–body models was done using the same setup as the wind-tunnel test using a simple chamber.

D. Experimental Conditions

The cylinder model tests were conducted for the three test cases shown in Table 2. In each case, the model was repainted and a new layer of TSP was formed, so that a range of layer thickness from 0.2 to 3 μm could be covered in each of the three cases. For each case, the measurements were repeated three times to evaluate the repeatability of the measurements.

The wing–body model tests were conducted for the six cases as shown in Table 3. In the first case, the angle of attack, α, was set to zero. The global heat flux distribution overall wing–body model was measured by TSP and compared with a schlieren photograph. For cases 2–6, the angle of sideslip, β, varied from 0 to 30 deg, while the angle of attack was kept at 0 deg.

E. Data Processing

The wind-off reference image, I_{ref}, was taken just before every shock tunnel run. Twenty images were acquired as a reference and averaged to reduce the shot and readout noise. Sequential 103 wind-on images were taken during flow duration by triggering the camera with an output signal from the pressure transducer located just upstream of the second quick valve. Both the wind-off reference images and wind-on shot images were compensated for dark images. The reference temperature was measured by a resistance temperature detector attached to the back of the model. Before calculating the image ratio, I/I_{ref}, the spatial filter was applied to both the wind-on and wind-off images to reduce noise. The image ratio, I/I_{ref}, was calculated after these treatments. Then, the image ratio, I/I_{ref}, was

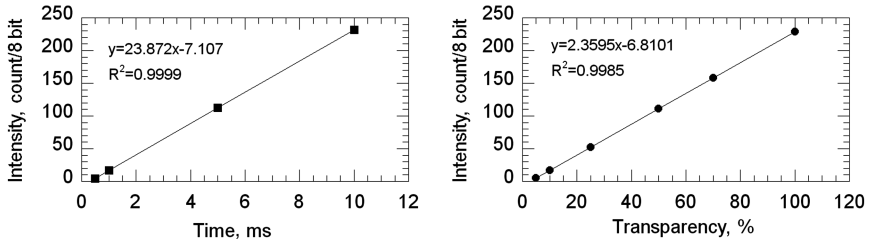

a) b)

Fig. 14 Linearity in the intensity of our fluorescence capturing systems of the neutral density filter: a) for exposure time, and b) for transparency time.

[¶]Data available online at http://www.shimadzu.com/products/test/hsvc/oh80jt0000001d6t.html [retrieved 1 May 2008]

Table 2 Experimental conditions of TSP thickness for cylinder model tests

	Location		
Case	A, μm	B, μm	C, μm
1	0.8 ± 0.2	1.3 ± 0.4	1.9 ± 0.4
2	0.2 ± 0.1	1.6 ± 0.3	2.5 ± 0.4
3	0.5 ± 0.2	1.0 ± 0.4	1.2 ± 0.5

Table 3 Experimental conditions for the wing–body model tests

Case	Contents	α, deg	β, deg
1	Overall model		0
2			0
3			10
4	Leading edge of model	0	15
5			20
6			30

transformed to the final temperature image using the calibration data of Eq. (5). The spatial filter was used on this sequence again.

V. Results and Discussions

A. Cylinder Model

Figure 15 shows the sequential temperature distributions of the cylinder model for case 1. The surface temperature at the stagnation line increased rapidly as it was heated in hypersonic flow. The magnitude of the temperature rise (ΔT) was different among TSP layers with different thicknesses and increased as the TSP layer became thicker. Figure 16 shows the typical temperature history at the stagnation point for the various TSP thicknesses of 0.2, 0.8, and 2.5 μm. In this graph, the temperature histories of the TSP were compared with those of the thin thermocouples. The horizontal axis is the time after heating starts and the vertical axis is the temperature rise from a steady state. The difference between the TSP measurement and the thin thermocouple data increased as TSP layer thickness increased. The difference was the largest for $h = 2.5$ μm. However, the difference was negligible for $h = 0.2$ μm.

Figure 17 shows the relationship between the TSP layer thickness and the temperature difference in all of the cases. The horizontal axis represents the thickness of the TSP layer. The vertical axis is the ratio of the temperature rises measured by TSP and the thin thermocouple (ΔT_{tc}). The solid line represents the CFD results for the simple heat conduction model, as shown in Fig. 3. The experimental data agreed well with the simple model for a thin TSP thickness, but they deviated from the simple model as the paint thickness increased. Two reasons were offered to account for this discrepancy. First, there is a possibility that the semi-infinite model will not work for a long-duration measurement (30–50 ms) such as the present experiment. However, it is understood that the distance to which the heat

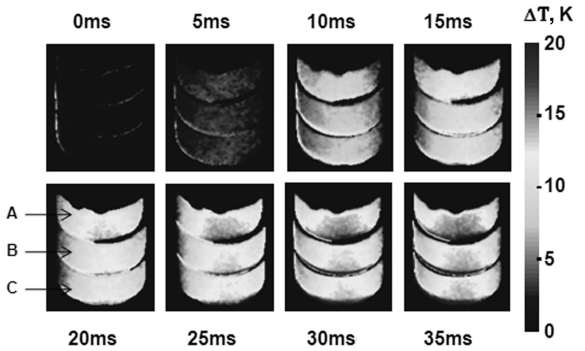

Fig. 15 Sequential temperature distributions of the cylinder model for case 1.

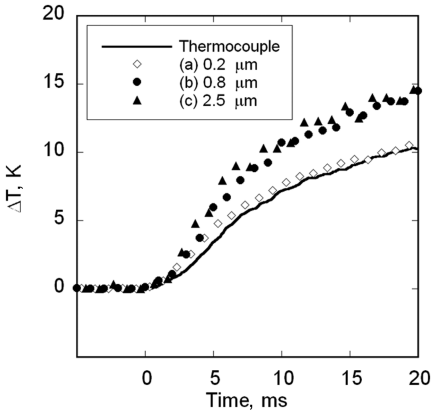

Fig. 16 Temperature increase history at the stagnation point.

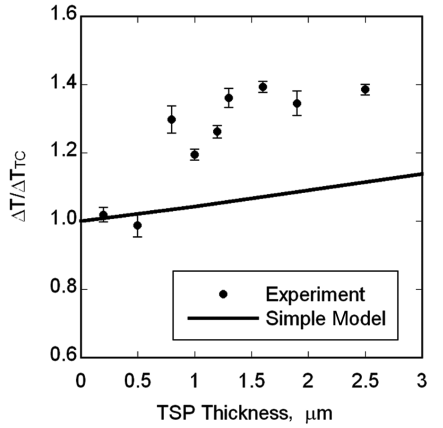

Fig. 17 Temperature error between the TSP and thermocouple as a function of TSP thickness.

penetrated the model was only about 0.6 mm at 30 ms, because the ceramic has a very high thermal insulating property. Therefore, it is thought that the semi-infinite model was appropriate in the present case. However, it is thought that the thermal property of TSP used by the model was not appropriate for the present test. In computation, the typical polymer properties ($\kappa = 0.2$ W/(m · K), $c = 1.2$ kJ/(kg · K), and $\rho = 1200$ kg/m^3) were used for the TSP. However, there are no data for the actual TSP, and it was different from the physical properties' values for a mere polymer because of a porous quality, which meant that the discrepancy of the data became larger. Moreover, the surface roughness also became larger as the TSP layer thickness increased. Furthermore, the thermal resistance of the porous media was also larger than that of the homogeneous surface because it had air in the hole and any bonding was insufficient. Accordingly, it was thought that the difference in the thermal conductivity for the experimental results and computation results caused a large error. However, the purpose of this paper was to determine a film thickness that can be used within a practical range. From such a viewpoint, the results showed that, to keep the TSP error in a temperature smaller than 2%, the thickness of the TSP layer should be kept at less than 0.5 μm.

Figure 18 shows the heat flux history calculated from the temperature data in Fig. 15 and using Eq. (9). Letters a, b, and c corresponded to the data for a TSP layer thicknesses of $h = 0.2$, 0.8, and 2.5 μm, respectively. For $h = 0.2$ μm, the time variation of heat flux measured by the TSP was the same as the thin thermocouple data. However, for the cases of $h = 2.5$ μm, the heat flux measured by the TSP was about 1.5–1.7 times larger than that measured by the thin thermocouple. Such large errors are not acceptable for practical wind-tunnel tests. Thus, it was concluded that, to make an accurate heat transfer measurement using the TSP, the thickness of the TSP layer must be kept smaller than about 0.5 μm.

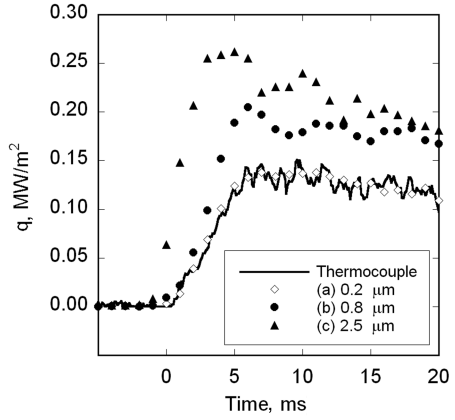

Fig. 18 Comparison of heat flux measured by the TSP and thermocouple.

B. Wing–Body Model

To demonstrate the validity of using TSP for accurate heat transfer measurement in practical tests, the TSP technique was applied to the testing of the wing–body model. The discussion in the previous sections suggested that the thickness of the TSP layer must be kept smaller than 0.5 μm to ensure accurate heat transfer measurement and practical use. Therefore, when we applied TSP on the wing–body model, the TSP layer thickness was kept at 0.2 μm. Figure 19a shows a schlieren photograph of the wing–body model. However, Fig. 19b shows the heat flux distribution over the model as measured by the TSP for case 1. These results were obtained by integrating the temperature data over a period of 10 ms starting from $t = 5$ ms. It is evident in Fig. 19a that shock wave/shock-wave interaction occurred at the wing's leading edge. A bow shock propagated from the model nose was an incident against a shock wave generated along the wing's leading edge. This is a shock wave/shock-wave interaction designated by Edney [18] as a *type VI*, in which expansion waves generated from the interacting point entered into the wing's leading edge. In Fig. 19b, it is evident that the region of the nose and leading edge were intensely heated. The nose was a stagnation region and subject to higher heat flux than other regions. The heated region of the leading edge in Fig. 19b was the same as the region of the shock wave/shock-wave interaction in Fig. 19a. Therefore, this heat flux was considered to be attributed to the shock-wave interaction.

A variation of the global heat flux pattern along the wing's leading edge for different β was investigated to discuss the effect of shock wave/shock-wave interactions on aerodynamic heating. Figure 20 shows a photograph of the experimental setup for the wing–body model for cases 2–6. Figure 21 shows the time-averaged heat flux result for the wing–body model for 20 ms. The peak heat flux region moved forward and the heating region increased as β increased. Figure 22 is the heat flux profile around the leading edge for cases 2–6. The horizontal axis is the distance from the leading edge. The peak heat flux increased and the width of its region became narrow as β increased. The peak heat flux in the case of $\beta = 30$ deg became the highest among all of the cases. The value was about two times higher than the case of $\beta = 0$ deg. It is considered that the intense heat flux was not attributed to the shock/shock-wave interaction of a *type VI* but was impinging on the hot jet gas generated from the shock/shock-wave interaction of a *type IV*.

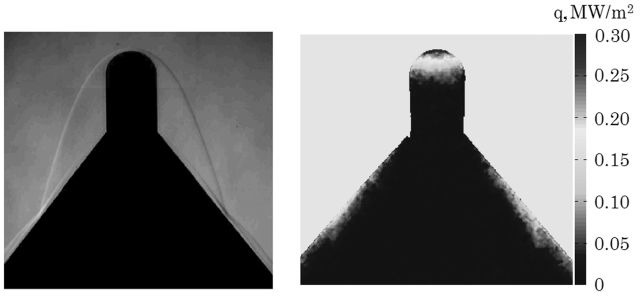

Fig. 19 Comparison the flowfield of the schlieren photograph with heat flux distribution: a) schlieren photograph of the wing–body model, and b) time-averaged heat flux image.

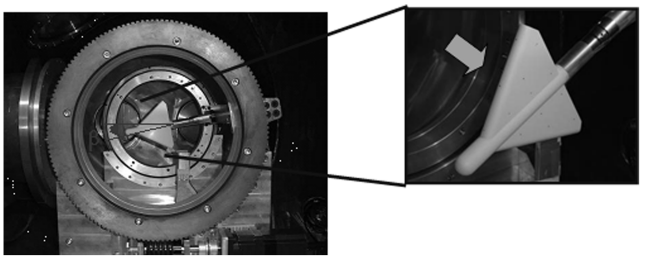

Fig. 20 Photograph of the experimental setup for the wing–body model with the case of an increasing sideslip angle of β.

VI. Conclusions

In the present study, the heat flux distribution caused by the aerodynamic heating of hypersonic flow was measured using the TSP technique to investigate the optimal TSP layer thickness in terms of measurement accuracy and the signal-to-noise ratio. A TSP with an optimal layer thickness was applied during the tests using a three-dimensional wing–body model having a complicated shapes to

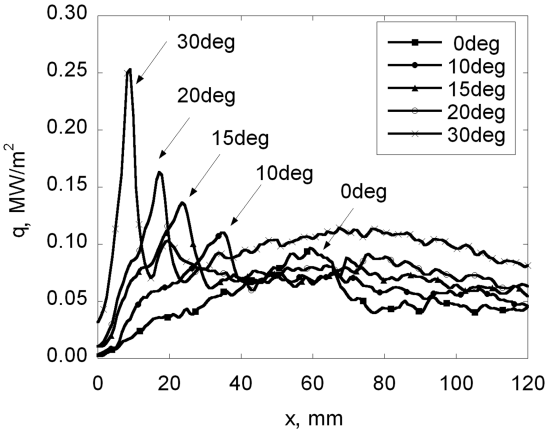

Fig. 22 Heat flux profile around the leading edge.

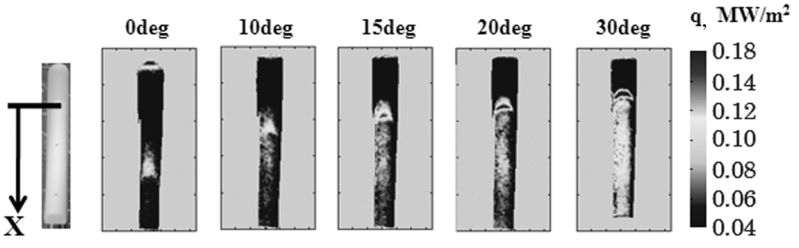

Fig. 21 Heat flux distributions around the leading edge.

evaluate the capability. It can be concluded that the TSP with a dye concentration of 10^{-2} mol/l was found to be the most suitable from the viewpoint of measurement accuracy, and the accuracy of the heat flux measurement by TSP was within the uncertainty of the conventionally thin thermocouples for a TSP layer thickness of 0.2 μm. Furthermore, complicated heat flux patterns caused by shock wave/shock-wave interaction on a three-dimensional wing–body model could be visualized using TSP, which demonstrated the validity for accurate heat transfer measurement in practical tests.

Acknowledgments

We wish to thank M. Watari, S. Tsuda, K. Mituo, K. Morita and Y. Iijima at the Japan Aerospace Exploration Agency for their technical support for experimental work in shock tunnel tests. We also thank our research group member, Y. Ishiguro for his personal support and technical discussion.

References

[1] Cook, W. J., and Felderman, E. J., "Reduction of Data from Thin Film Heat Transfer Gauges—A Concise Numerical Technique," *AIAA Journal*, Vol. 4, No. 3, 1966, pp. 561–562.

[2] Schults, D. L., and Jones, T. V., "Heat-Transfer Measurements in Short-Duration Hypersonic Facilities," AGARD Paper AG-165, Feb. 1973.

[3] Jagadeesh, G., Reddy, K. P. J., Hashimoto, T., Naitou, K., Sun, M., and Takayama, K., "Study of the Separated High Enthalpy Flow Around a Double Cone," AIAA Paper 2002-229, 2002.

[4] Buck, G. M., "Surface Temperature/Heat Transfer Measurement Using a Quantitative Phosphor Thermography System," AIAA Paper 1991-64, 1991.

[5] Balageas, D. L., Boscher, D. M., and Deom, A. A., "Measurement of Convective Heat-Transfer Coefficients on a Wind Tunnel Model by Passive and Stimulated Infrared Thermography," *Proceedings of SPIE*, edited by I. J. Spiro, Vol. 1341, International Society for Optical Engineering, Bellingham, WA, Nov. 1990, pp. 339–357. doi:10.1117/12.23107.

[6] Smith, A. J. D., and Baxter, D. R. J., "Liquid Crystal Thermography for Aerodynamic Heating Measurements in Short Duration Hypersonic Facilities," *Proceedings of Instrumentation in Aerospace Simulation Facilities 1989*, IEEE Publications, Piscataway, NJ, 1989, pp. 104–112. doi:10.1109/ICIASF.1989.77663.

[7] Liu, T., Campbell, B. T., Sullivan, J. P., Lafferty, J., and Yanta, W., "Heat Transfer Measurement on a Waverider at Mach 10 Using Fluorescent Paint," *Journal of Thermophysics and Heat Transfer*, Vol. 9, No. 4, 1995, pp. 605–611.

[8] Hubner, J. P., Carroll, B. F., Schanze, K. S., Ji, H. F., and Holden, M. S., "Temperature- and Pressure-Sensitive Paint Measurements in Short-Duration Hypersonic Flow," *AIAA Journal*, Vol. 39, No. 4, 2001, pp. 654–659.

[9] Hubner, J. P., Carroll, B. F., Schanze, K. S.,"Heat-Transfer Measurements in Hypersonic Flow Using Luminescent Coating Techniques," *Journal of Thermophysics and Heat Transfer*, Vol. 16, No. 4, 2002, pp. 516–522.

[10] Nakakita, K., Osafune, T., and Asai, K., "Global Heat Transfer Measurement in a Hypersonic Shock Tunnel Using Temperature-Sensitive Paint," AIAA Paper 2003-743, 2003.

[11] Nakakita, K., and Asai, K., "Method and Apparatus for Measuring Heat Flux Distribution on Object Surface Using Temperature-Sensitive Paint," US Patent No. US 7069169 B2, 2006.

[12] Nakakita, K., and Asai, K., "Method and Apparatus for Measuring Heat Flux Distribution on Object Surface Using Temperature-Sensitive Paint," Japan Patent No. 3704563, 2005.

[13] Liu, T., Campbell, B. T., Burns, S. P., and Sullivan, J. P., "Temperature- and Pressure-Sensitive Luminescent Paints in Aerodynamics," *Applied Mechanics Reviews*, Vol. 50, No. 4, 1997, pp. 227–246.

[14] Bell, H. J., Schairer, T. E., Hand, A. L., and Mehta, R. D., "Surface Pressure Measurements Using Luminescent Coatings," *Annual Review of Fluid Mechanics*, Vol. 33, Jan. 2001, pp. 155–206. doi:10.1146/annurev.fluid.33.1.155

[15] Anandan, C., and Basu, B. J., "Study of the Diffusion of Pyrene in Silicone Polymer Coatings by Steady State Fluorescence Technique: Effects of Pyrene Concentration," *European Polymer Journal*, Vol. 40, No. 8, 2004, pp. 1833–1840. doi:10.1016/j.eurpolymj.2004.03.024

[16] Hubner, J. P., and Carroll, B. F., "Application of Dual Sorption Theory to Pressure-Sensitive Paints," *AIAA Journal*, Vol. 35, No. 11, 1997, pp. 1790–1792.

[17] Liu, T., and Sullivan, J. P., *Pressure and Temperature Sensitive Paints*, Springer–Verlag, Berlin/Heidelberg/New York, 2004, pp. 169–170.

[18] Edney, B., "Effects of Shock Impingement on the Heat Transfer Around Blunt Bodies," *AIAA Journal*, Vol. 6, No. 1, 1968, pp. 15–21.